Unlocking Emerging Impacts of Carbon Tax on Integrated Energy Systems through Supply and Demand Co-optimization ✧

Meng Wang [a, b], Hang Yu [a] * ✉, Yikun Yang [a], Xiaoyu Lin [a], Haijin Guo [a], Chaoen Li [a], Yue Zhou [c], Rui Jing [c] * ✉

a School of Mechanical Engineering, Tongji University, Shanghai, China
b Department of Civil Engineering, Technical University of Denmark, Kgs. Lyngby, Denmark
c School of Engineering, Cardiff University, Cardiff, UK

Abstract: Integrated energy systems (IES) can help achieve greater energy efficiency, and then ultimately promote a climate-neutral economy by utilizing local renewable resources. Demand-side energy-saving measures can reduce operational costs associated with energy usage. Most existing IES models, however, focus on supply-side optimization, while the demand-side energy-saving potential and its impacts on whole-system performance are still not clear. The increasing carbon tax makes it even more important to understand the interactions between supply and demand sides to achieve a sustainable system with a minimal carbon charge. Hence, this study proposes a co-optimization model to simultaneously optimize the supply and demand sides of an IES considering the impact of the carbon tax. A selection tree is developed to describe various demand-side envelope upgrading technologies, and a binary tree is established by generating a set of supply-side scenarios with corresponding probabilities. Based on these results, an improved two-stage stochastic programming model is proposed. The robustness of the modeling results was further validated by a simulation-optimization-based uncertainty analysis addressing price uncertainties. A case study in Shanghai indicates that the proposed co-optimization model achieves more cost-efficient solutions than supply-side-only optimization considering carbon tax. Introducing carbon tax can reduce the installed capacity of fuel-based energy technologies by up to 24% and greatly accelerate the penetration of renewables. The increasing carbon tax also promotes the adoption of more advanced energy-saving technologies. Uncertainty analysis reveals acceptable robustness of the optimal demand-side scheme and supply-side configuration with a deviation of less than 5% and a coefficient of variation of 7%. Overall, the observations of the proposed model and case study provide valuable insights for IES design considering an emerging charge of carbon tax.

Keywords: Integrated energy system; supply and demand-side co-optimization; carbon tax; stochastic programming; uncertainty analysis.

---

* Corresponding author.
E-mail ✉: tjyuhang@163.com (H. Yu), fafujingrui@126.com (R. Jing)

✧ The short version of the paper was presented at ICAE2020, Dec. 1–10, Bangkok, Thailand. This paper is a substantial extension of the short version of the conference paper.

Nomenclature

Abbreviations		*CAT*	Carbon tax
B	Basic envelope upgrading	*L*	Energy demand (kW)
CAPEX	Capital cost	*NG*	Heating value of natural gas
CEEX	Carbon emission cost	*Obj*	Objective
CHP	Combined heat and power	*prob*	Scenario's probability
CRF	Capital recovery factor	*Q*	Energy supply (kW)
CV	Coefficient of variation	*r*	Interest rate
DF	Discount factor	*y*	Project year
FC	Fuel cost	*Greek symbols*	
FIT	Feed-in tariff	γ	Startup time
GC	Electricity purchased cost	ζ	Binary variable
IES	Integrated energy system	η	Efficiency
INV	Investment cost	λ	Carbon emission factor
MC	Maintenance cost	φ	On/off status
MILP	Mixed-integer linear programming	*Subscripts/superscripts*	
N	None envelope upgrading	ac	Absorption chiller
OPEX	Operation cost	b	Gas boiler
P	Premium envelope upgrading	ec	Electrical chiller
PV	Photovoltaic panel	ex	Electricity export
REP	Replacement and maintenance cost	*h*	Time step (hour)
S	Standard envelope upgrading	hp	Air source heat pump
SHGC	Solar heat gain coefficient	hs	Heat storage
SRI	Solar radiation intensity	hs-in	Heat storage charge
STD	Standard deviation	hs-out	Heat storage discharge
TAC	Total annual cost	im	Electricity import
TOU	Time of use	k	Energy technology
UC	Unit cost	max	Maximum
UPEX	Upgrading cost	maint	Maintenance cost
XPS	Extruded polystyrene	min	Minimum
Symbols		s	Supply-side scenario
CAP	Installed capacity (kW)	t	Demand-side scenario

1. Introduction

By integrating clean energy options, such as solar energy, wind energy, biomass energy, and geothermal energy, integrated energy systems (IES) can effectively improve the whole-system efficiency and power a climate-neutral economy [1]. The European Commission has agreed that IES lays a pathway toward a more effective, affordable, and decarbonized European economy [2]. However, the integration of multiple energy carriers and technologies has led to significant challenges in coordinated planning and operation. Hence, researchers are increasingly focusing on optimal system design or dispatch strategies for IES.

Owing to the improvement of computational resources and mathematical programming modeling techniques, the modeling of IES has become increasingly comprehensive in order to integrate all of the available energy techniques into IES models [3]. The optimal system configurations and dispatch strategies should not only be achieved on the supply side but also on the demand side, to integrate energy-saving technologies into IES models. This will further improve the performance of energy systems, especially considering the carbon tax. This study presents a co-optimization model to incorporate supply-side and demand-side energy technologies to achieve simultaneous optimization. An uncertainty analysis was then conducted to validate the robustness of the proposed model.

1.1 Modeling integrated energy system from the supply side

The application of optimization methods plays an influential role in helping decision-makers achieve the optimal design of an IES [4]. Among various optimization models, the indices describing economic performance are the most frequently used and fundamental objectives, such as the levelized cost of energy [5], total annual cost [6], operation cost (OPEX) [7], and total net present cost [8]. Mu et al. [9] proposed a decentralized optimization model for a small-sized IES to optimize its dispatch strategy, while the operation cost acted as the economic objective. The model was solved with good convergence performance using the alternating direction multiplier method (ADMM). Wu et al. [10] conducted a comparative study to optimize the operation

strategy for multi-scenario IES, including building and district scales. They presented a collaborative optimization method combining genetic algorithm and orthogonal experimental design to optimize the economic objective. The results showed that collaborative optimization performed better than non-collaborative optimization.

Economic factors contributing to IES costs generally include capital, operation, fuel, and maintenance costs. The carbon tax can also describe the environmental performance by combining it with economic indices [11]. Dorotic et al. [12] introduced a carbon tax and an exergy destruction tax to conduct a multi-objective optimization for district heating systems. Their study analyzed the impact of exergy tax on the natural gas consumption of a single-technology heating system, with the results indicating that the system's efficiency could be improved with an increase in the carbon tax. Martelli et al. [13] proposed a bi-level approach for multi-energy systems to mimic the actual bi-level decision process in order to optimize the renewable subsidy and carbon tax for IES. Based on four real-world case studies from the building scale to the district scale, their heuristic approach's effectiveness was verified.

Moreover, other studies considered some critical parameters as uncertain factors of IES and investigated their impacts on systems' economic and environmental performance. Mavromatidis et al. [14] applied uncertainty and global sensitivity analysis to identify the most influential parameters for all potential uncertain parameters. The results highlighted that the energy carrier price and energy demands have obvious influences on other factors. Furthermore, they proposed a two-stage stochastic programming approach to capture uncertain factors and optimize the system design with an economic objective [15]. The epsilon constraints and Pareto optimization were combined with a two-stage stochastic programming approach to deal with the multi-objective optimization problem of IES [16]. Their results in [15] and [16] both illustrated the significant influences of various prices on the system's economic performance and the optimal conservativeness of the design considering uncertainties. All these studies have made pioneering efforts in modeling the supply-side configuration without any upgrading of the demand side, which may further improve the performance of IES.

1.2 Integrated optimization of energy supply and demand

Studies tend to apply various optimization methods to solve optimal solutions for the energy demand side, including building envelope upgrading and demand response, which can also be simplified as energy-saving [17] and load transfer technologies [18]. Liu et al. [19] conducted a cost-benefit analysis of building envelope upgrading through a real-world residential district project, which involved the upgrade of windows and external walls. The analysis of the measured data highlighted that selecting upgraded materials significantly impacts economic outcomes and energy-saving performance. For public buildings, Wang et al. [20] introduced a quantum genetic algorithm to optimize the office building envelope design, including the window area, glass curtain wall ratio, and external wall. The results showed the beneficial effects of the design optimization model on the building performance so that the total cost could be decreased by a third when compared to the original design. Chang et al. [21] applied a multi-objective optimization model to the selection of emerging materials and technologies for improving indoor thermal comfort, environmental emissions, and economic aspects, providing decision support for transforming the performance of existing buildings.

Although many studies have made significant efforts to pursue the optimal decision of demand-side design, less attention has been paid to combining supply-side and demand-side models to implement simultaneous optimization. A few representative studies have attempted to bring the optimal selection of building energy-saving technologies into IES models from a centralized planning perspective, which could obtain better overall system performance. Zheng et al. [22] presented an optimization-based planning model for urban energy systems integrating optimal supply- and demand-side technology portfolios. In their model, the demand-side model was developed as a simplified heat transfer process, and the results provided the optimal configuration, dispatch, and upgrading scheme (including exterior walls, windows, roofs, doors, and floors) for their case. Ferrara et al. [23] proposed a building-scale co-optimization model to investigate a multi-family building case and provide optimal solutions for integrating measures for building envelopes and energy systems. The

results demonstrated that the co-optimization model could generate more possible combinations of energy technologies than sequential optimization. Moreover, other factors of the demand side can also be considered to be combined with supply-side modeling, as reported by Perera et al. [24] for integrating urban morphology and Liu et al. [25] for integrating demand response. Many studies have explored the feasibility and effectiveness of supply- and demand-side co-optimization via an integrated framework to simultaneously obtain optimal designs. The demand-side modules, however, were simple when compared with the corresponding supply-side module. Possible difficulties may lie in matching various modeling scales and coupling building energy formulas with mathematical programming models.

1.3 Motivation and contribution

The literature review highlights that existing studies tend to optimize the IES model from the supply and demand sides in a separate way. The potential of supply-demand co-optimization to improve the whole-system performance, as well as the impact of carbon tax, has not been well explored. Meanwhile, the co-optimization model usually involves numerous scenarios with high dimensionality, and thus it is challenging to formulate a computationally traceable and robust model.

This study develops a co-optimization IES model to optimize the decisions on envelope upgrading technologies, system configurations, and dispatch strategy simultaneously by coupling the supply-side and demand-side modules. The impact of carbon tax on optimal decisions was assessed, and the robustness of the optimal decisions was further validated by a simulation-optimization-based uncertainty analysis. The contributions of this study are as follows.

- ➢ Explicitly simulate energy-saving effects for *Basic*, *Standard*, and *Premium* levels of envelope upgrading on external walls, roofs, and windows, and then develop a comprehensive tree for selecting optimal demand-side upgrading schemes.

- ➢ Propose an improved two-stage stochastic co-optimization model to integrate the supply-side and demand-side modules, and then unlock the impact of carbon

tax on optimal design of IES.

➢ Validate the robustness of optimal decisions obtained by the co-optimization model based on an uncertainty analysis addressing various prices.

The rest of the paper is organized as follows: Section 2 illustrates the outline and methodology. Section 3 introduces a case study to apply the proposed co-optimization model, and the results are analyzed and discussed in Section 4. Several key conclusions are presented in Section 5.

2. Methodology

Fig. 1 illustrates the outline of the present study, which can be divided into four major parts: (A) demand-side scenario generation, (B) supply-side scenario generation, (C) IES design modeling, and (D) uncertainty analysis. In step (A), the building envelope upgrading scheme is considered as the decision variable to be optimized in the co-optimization model. Meanwhile, a demand-side selection tree is introduced to describe a series of alternative envelope upgrading technologies for external walls, roofs, and windows. In step (B), the clustering method is applied to generate the supply-side binary tree in order to capture the variations in energy demands and renewable resources. Both the supply-side and demand-side scenario trees were constructed layer-by-layer to consider each critical factor in the proposed model. In step (C), a mixed-integer linear programming (MILP)-based IES planning model is developed to incorporate the supply-side and demand-side scenarios into one co-optimization model to simultaneously optimize the system design, including capacity configuration, dispatch strategy, and envelope upgrading scheme. In particular, the impact of the carbon tax on the system design is evaluated. In step (D), an uncertainty analysis method combining Monte Carlo simulation and operation optimization was adopted to validate the robustness of the modeling results considering different price uncertainties. The methods are described in the following subsections.
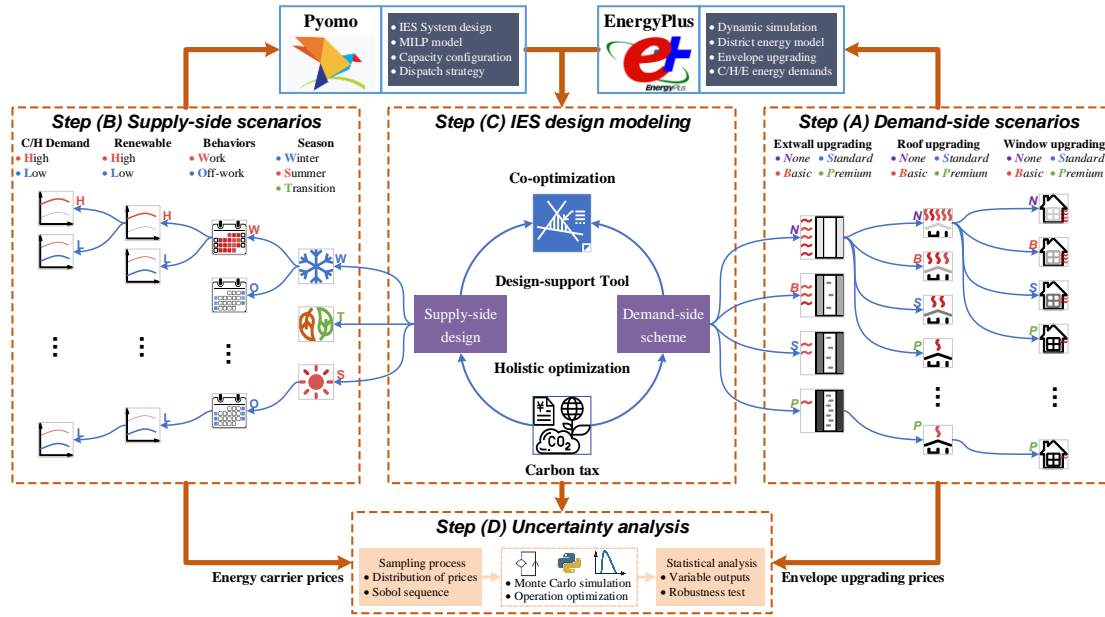
Fig. 1. Outline of the proposed work for co-optimization of IES.

2.1 Demand-side scenario generation

The hourly energy demands of the district are projected by building performance simulations according to local climate conditions. Local meteorological data were acquired from the China Integrated Meteorological Information Sharing System (CMISS) and fed to the EnergyPlus building energy simulation tool to obtain the whole-year hourly resolution electrical, heating, and cooling demands. The window-wall ratio, ventilation, occupant behavior, occupant density, and internal disturbance are considered in the building energy simulation, which is based on the design standard for energy efficiency of residential buildings [26] and design standard for energy efficiency of public buildings [27].

The building envelope upgrading scheme acts as an energy-saving technology in the present study by varying the thermal properties of external walls, roofs, and windows. Compared with the uncertainties of other factors affecting the energy demands of buildings, envelope construction can be designed and determined at the planning stage, and its properties are fairly stable during the planning period [28]. Hence, this study introduced four upgrading levels for each alternative envelope upgrading: *None*, *Basic*, *Standard*, and *Premium*. For the construction of external walls and roofs, *None* indicates that the external wall (from outside to inside) has polymer mortar, cement mortar, perforated concrete brick, mixed mortar for external wall,

aggregate concrete, waterproof modified asphalt, cement mortar, and steel-reinforced concrete, but without an insulation layer [29][30]. Other upgrading levels (i.e., *Basic*, *Standard*, and *Premium*) refer to the extruded polystyrene (XPS) insulation layer with different thicknesses [31]. Meanwhile, energy-saving technologies of windows, for example, low-e, filling noble gas, and increasing layers, are introduced to generate the four window-upgrading scenarios [32]. The sketch diagrams for the external walls, roofs, and windows are shown in Fig. 2.
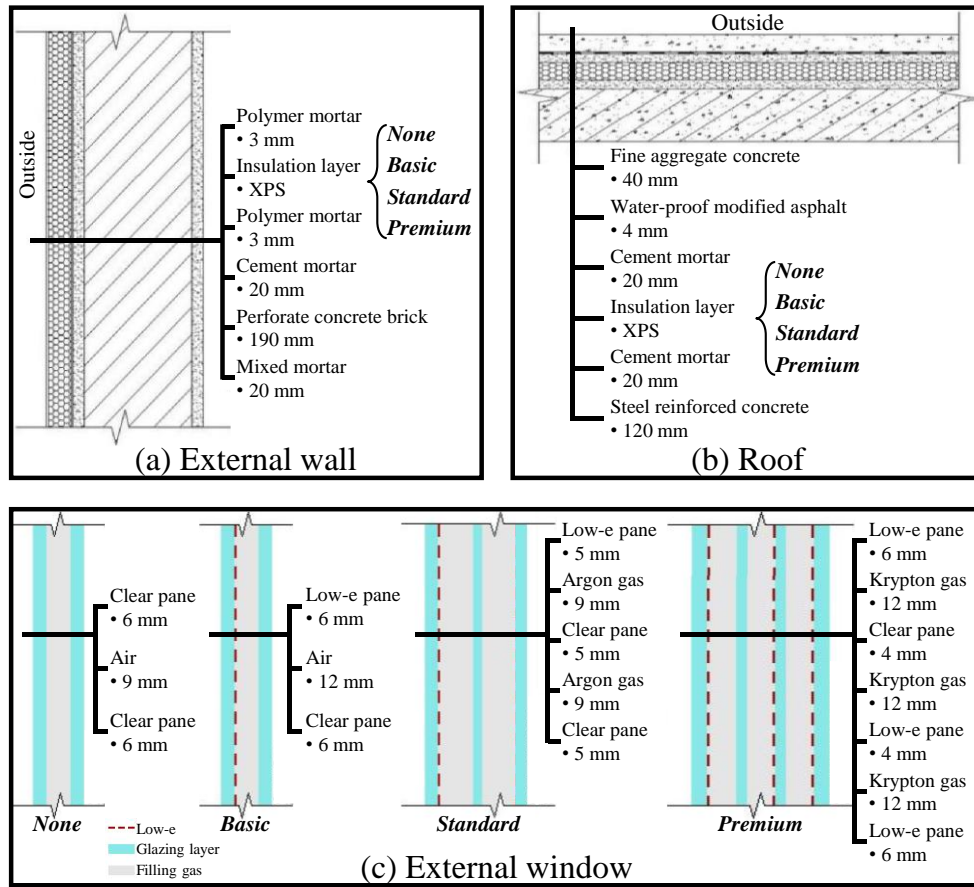
Fig. 2. Construction of external walls (a), roofs (b), and external windows (c) with their corresponding upgrading scenarios including *None*, *Basic*, *Standard*, and *Premium*.

The upgrading cost (UPEX), including investment (INV) and replacement and maintenance (REP), is accounted for in the co-optimization model [19]. The *Basic*, *Standard*, and *Premium* levels are associated with upgrade costs, while zero upgrade costs are associated with the *None* level. The investment cost of upgrading external walls and roofs can be calculated proportionally to the thickness of the insulation layers as an independent variable [23] defined in Eq. (1).

$$UPEX = \sum_t \left(\zeta_t^{\text{demand}} \times INV_t \times CRF^{\text{upgrade}} \right) + \sum_t \left(\zeta_t^{\text{demand}} \times REP_t \times DF^{\text{replace}} \times CRF^{\text{replace}} \right) \quad (1a)$$

$$INV_t^{\text{env}} = \sum_{e \in \{\text{wall,roof}\}} \left(UC_{t,e}^{\text{init}} + UC_{t,e}^{\text{insulation}} \times \left(\delta_{t,e}^{\text{insulation}} - \delta^{\text{init}} \right) \right) \times AREA_e \quad (1b)$$

$$REP_t = Ratio^{\text{replace}} \times INV_t \quad (1c)$$

$$DF = \frac{1}{(1+r)^y} \quad (1d)$$

$$CRF = \frac{r \times (1+r)^y}{(1+r)^y - 1} \quad (1e)$$

where DF is the discount factor, CRF is the capital recovery factor, UC is the unit cost of envelope upgrading, and the subscripts e and t indicate the envelope and demand-side scenario, respectively. The superscript $init$ represents initial cost. Note that the initial cost includes the cost of a basic 25 mm insulation layer. The $Ratio^{\text{replace}}$ indicates the ratio of the replacement cost to its corresponding investment cost.

Table 1 reports the details of each envelope upgrading scenario, including the economic parameters and calculated thermal properties.

Table 1 Detailed information on envelope upgrading technologies.

Item	Unit	External wall			Roof			Window		
		Basic	*Standard*	*Premium*	*Basic*	*Standard*	*Premium*	*Basic*	*Standard*	*Premium*
Initial cost	$/m²		25.25			26.77		42.43	55.08	121.22
Insulation cost	$/m²	1.85 (per 5 mm thickness)			2.08 (per 5 mm thickness)					
$Ratio^{\text{replace}}$	-		0.2			0.2			0.2	
δ^{init}	mm		25			25			-	
$\delta^{\text{insulation}}$	mm	25	45	100	25	55	100	-	-	-
U-value	W/m²K	0.91	0.56	0.28	1.02	0.51	0.29	1.9	1.2	0.43
SHGC	-	-	-	-	-	-	-	0.46	0.46	0.37
Life cycle	year					30				
Replacement	year					15				

Finally, the demand-side scenarios are organized according to the various upgrading schemes of envelopes, including four levels for external walls, four levels for roofs, and four levels for windows. Therefore, 64 demand-side scenarios were generated as a selection tree. These demand-side scenarios are mutually exclusive, and only one scenario can be selected from the structure, as expressed in Eq. (2). If needed (e.g., for optimizing operation only), decision-makers can predefine the binary variable

ζ to control the implementation of envelope upgrading technologies of the demand-side module.

$$\sum_{t} \zeta_{t}^{\text{demand}} = 1 \tag{2}$$

where the subscript t denotes the demand-side scenarios.

2.2 Supply-side scenario generation

Introducing whole-year hourly data, including renewable resources and energy demands, into the optimization model may generate a considerable number of variables and constraints, which may lead to a high-dimensional problem and an unacceptable computational cost. The global optimum is hardly guaranteed even if the high-dimensional optimization model can be solved. Hence, for ensuring computational traceability, this work proposed a scenario generation method to generate a series of stochastic scenarios for capturing the whole-year variations and then introduced them, rather than the whole-year hourly data, into the proposed co-optimization model. Fig. 3 illustrates the stochastic-scenario-based binary tree developed by using clustering-based classification methods. The *K*-medoids algorithm is applied, which has better performance on time-series energy consumption data [33]. The probability of each cluster is equal to the ratio of the number of individuals belonging to it to the total number of individuals [16].
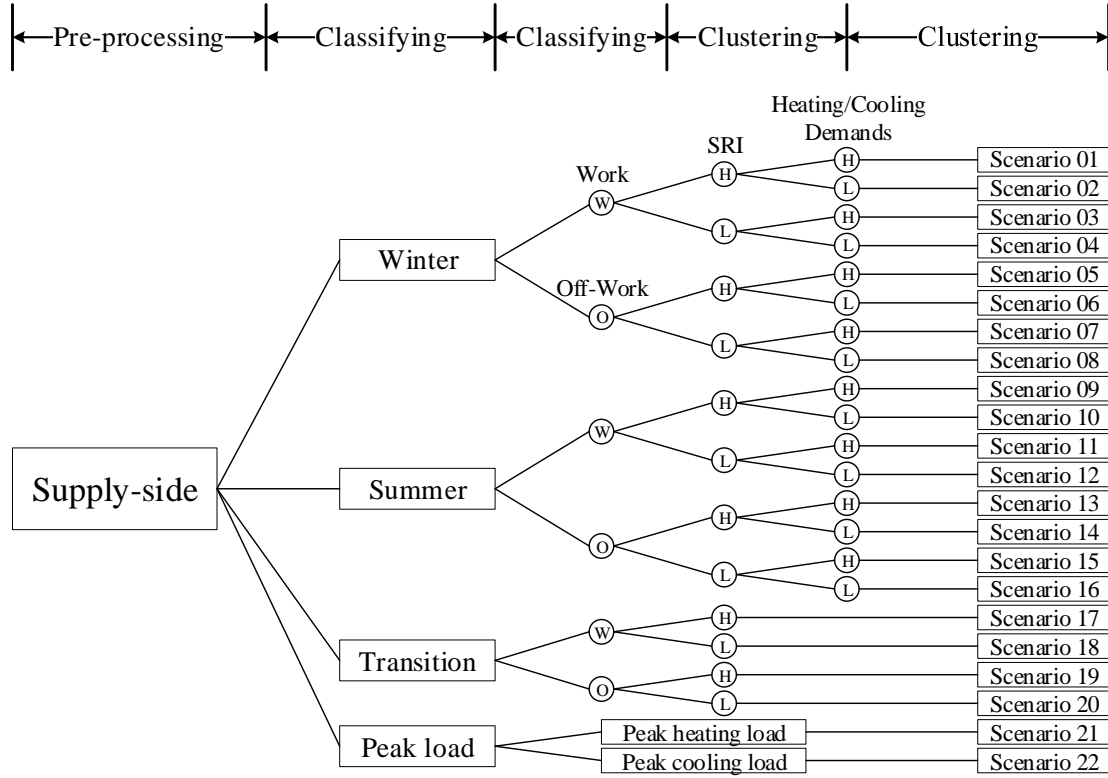
Fig. 3. Diagrammatic sketch of stochastic-scenario-based binary tree for supply side.

Before the clustering layers, two classification layers were constructed considering different seasons as well as the work/off-work duality. Moreover, two additional scenarios were introduced to describe the peak load scenarios with maximum heating demand and maximum cooling demand. Overall, the entire scenario tree has 22 stochastic scenarios to represent the whole-year demand and solar radiation fluctuations. For each scenario, the probability is assigned as the product of the probabilities of their corresponding intermediate scenarios in each layer, and the summation of each scenario's probability should be equal to one, as shown in Eq. (3).

$$\sum_s Prob_s^{supply} = 1 \tag{3}$$

where $Prob_s$ indicates the probability of s supply-side scenario.

2.3 Stochastic programming based co-optimization for supply and demand sides

This study proposes the co-optimization model for IES from a whole-system perspective, where the IES planner could make decisions on the design for both supply side and demand side, aiming to find the two-side global optimum solution taking the whole-system profit into account. Hence, the supply side and demand side are coordinated and represented by corresponding decision variables in one programming

model and optimized simultaneously.

Meanwhile, according to the scenarios developed above, the two-stage stochastic programming method was introduced to integrate them into one co-optimization model. Eq. (4) illustrates the general formulations for the energy-planning problem. The first-stage decision variables describe the system design, whereas the second-stage decision variables represent the time-series operation decisions. The total objective is equal to the summation of the expected values of the design and operation parts [34].

$$Obj^{\text{total}} = obj^{\text{design}} + \sum_{s=1}^{N} prob_s \times obj_s^{\text{operation}} \quad \forall s$$

$$\underbrace{\boxed{\text{Capacity-determing}} \quad \boxed{t \mid t+1 \mid t+2 \mid \cdots} \quad \text{Dispatch \& Operation}}_{\substack{\text{First-stage decision} \\ \text{Design variable}} \qquad \substack{\text{Second-stage decision} \\ \text{Operation variable}}} \tag{4}$$

Hence, the objective's expression needs to be modified to incorporate both the demand-side and supply-side scenarios into an integrated objective function, as shown in Eq. (5).

$$Obj = obj^{\text{design}} + \sum_{t} \zeta_t^{\text{supply}} \times obj_t^{\text{upgrade}} + \sum_{s} prob_s^{\text{demand}} \times obj_s^{\text{operation}} \tag{5}$$

2.4 Model description of IES

Fig. 4 illustrates the proposed IES superstructure considering a series of energy-supply technologies and demand-side envelope upgrading technologies to fulfill electricity, cooling, and heating demands simultaneously, modified from the previous study [28]. Moreover, the stochastic programming based co-optimization model, including various supply and demand-side scenarios, could cause high-dimensional problems with overlong solving time [35]. By contrast, meta-heuristic algorithms perform well in solving stochastic programming models, whereas the global optimum cannot be guaranteed [36]. Hence, all the objectives and constraints of the proposed co-optimization model are formulated in linear form with continuous and integer variables, i.e., a mixed-integer linear programming (MILP) model, which can be solved by calling state-of-the-art commercial solvers. The objective function and constraints are given in the following subsections and in **Appendix A**.
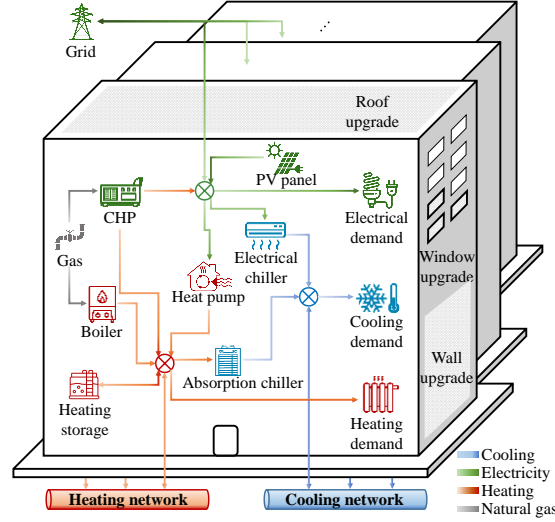
Fig. 4. Superstructure of the proposed IES with state-of-the-art technologies.

2.4.1 Objective function

Based on the formulation of Eqs. (4) and (5), the total annual cost (TAC) is defined by Eq. (6) to represent the life-cycle cost of a system that considers the carbon tax. Thus, TAC consists of four main parts: capital cost (CAPEX), upgrade cost (UPEX), operation cost (OPEX), and carbon emission cost (CEEX). The expressions of UPEX are described in Section 2.1. CAPEX represents the amortization of supply-side technologies' investment, while the OPEX is equal to the sum of the fuel cost (FC), maintenance cost (MC), and cost of electricity purchased from the bulk grid (GC), minus the income of the feed-in tariff (FIT). CEEX includes the capacity and operation parts [37]. The capacity part is equal to the summation of all energy-supply technologies' life-cycle carbon emissions (including raw material, manufacturing, installation, and disposal) [38], while OPCE denotes the carbon emissions of fuel consumption and electricity purchased for the bulk grid during the operation period.

$$TAC = UPEX + CAPEX + OPEX + CEEX \tag{6a}$$

$$CAPEX = \sum_k CAP_k \times UC_k^{cap} \times CRF^{supply} \tag{6b}$$

$$OPEX = \sum_s \left(\sum_h \left(FC_{s,h} + MC_{s,h} + GC_{s,h} - FIT_{s,h} \right) \times num^{day} \right) \times prob_s \tag{6c}$$

$$FC_{s,h} = \left(\frac{Q_{chp,s,h}^{ele}}{\eta_{chp}^{ele}} + \frac{Q_{b,s,d,h}^{heat}}{\eta_b} \right) \times UC^{NG} \tag{6d}$$

$$MC_{s,h} = \sum_k \left(Q_{pv/chp,s,h}^{ele} + Q_{hp/b/hs,s,h}^{heat} + Q_{ec/ac,s,h}^{cool} \right) \times UC_k^{maint} \tag{6e}$$

$$GC_{s,h} = Q_{im,s,h}^{ele} \times UC_h^{im} \tag{6f}$$

$$FIT_{s,h} = Q_{ex,s,h}^{ele} \times UC_h^{ex} \tag{6g}$$

$$CEEX = \left(\sum_k CAP_k \times \lambda_k^{cap} \times CRF^{supply} + OPCE \right) \times CAT \tag{6h}$$

$$OPCE = \sum_s \left(\sum_h \left(\lambda_{grid} \times Q_{im,s,d,h}^{ele} + \lambda_{NG} \times \frac{Q_{chp,s,d,h}^{ele}}{\eta_{chp}^{ele}} + \lambda_{NG} \times \frac{Q_{b,s,d,h}^{heat}}{\eta_b} \right) \times num^{day} \right) \times prob_s \tag{6i}$$

where CAT is the carbon tax per unit emission, and the subscript k denotes the energy conversion technologies.

2.4.2 Model constraints

The energy balance expresses the energy demand of the district for electricity, cooling, and heating must be fulfilled for each time step h of each supply-side scenario s, as shown in Eq. (7). The constant efficiency of the designed network is introduced to express the transfer loss of heating energy in Eq. (7b). Moreover, the binary variable ζ is used to ensure that only one demand-side scenario can be selected. The remaining model constraints are presented in **Appendix A**.

$$\sum_t \zeta_t^{demand} \times L_{s,h}^{ele} = Q_{pv,s,h}^{ele} + Q_{chp,s,h}^{ele} + Q_{im,s,h}^{ele} - Q_{ec,s,h}^{ele} - Q_{hp,s,h}^{ele} - Q_{ex,s,h}^{ele} \tag{7a}$$

$$\sum_t \zeta_t^{demand} \times L_{s,h}^{heat} = \eta_{net} \times \left(Q_{chp,s,h}^{heat} + Q_{b,s,h}^{heat} + Q_{hs-out,s,h}^{heat} + Q_{hp,s,h}^{heat} - Q_{hs-in,s,h}^{heat} - Q_{ac,s,h}^{heat} \right) \tag{7b}$$

$$\sum_t \zeta_t^{demand} \times L_{s,h}^{cool} = Q_{ac,s,h}^{cool} + Q_{ec,s,h}^{cool} \tag{7c}$$

2.5 Uncertainty analysis

Because the prices of energy carriers have a significant influence on the system economic performance [14], this study performs a Monte Carlo-based robustness analysis to investigate the system performance under various price uncertainties [16]. Six prices are considered as uncertain factors, including the ratio of the replacement cost to its corresponding investment cost for each envelope upgrading technology, the energy carriers' prices (i.e., natural gas and bulk grid), and the ratio of the FIT to purchased price from bulk grid. The uniform distribution is utilized to represent each uncertain factor's variation [34], as detailed in Table 2. Moreover, the Sobol sequence generator is used to obtain a well-distributed and high-quality sampling matrix with a lower computational cost, and all uncertain factors are assumed to be mutually independent [39]. More details of the Sobol sequence and Monte Carlo simulation can be found in Ref. [40].

Table 2 Price parameters of the deterministic condition and uncertain condition

Items	Deterministic condition		Uncertain condition
TOU electricity price	Peak:	0.203 $/kWh	
	Valley:	0.059 $/kWh	U[0.9, 1.1] × Deterministic
	Flat:	0.129 $/kWh	
Natural gas price		0.049 $/kWh	U[0.039, 0.059] $/kWh
Feed-in tariff ratio		0.83	U[0.66, 1] × Deterministic
Replacement cost ratio		0.2	U[0.1, 0.3]

2.6 Modeling environment

A computing server with Intel Xeon E31230 and 32 GB of RAM was used in this study. The building energy simulation was performed in EnergyPlus9.2 with its Python-based scripting language 'Eppy'. The clustering process and Monte Carlo simulation were both conducted in Python, while a Python toolbox, named 'Pyomo', was used to develop the two-stage MILP model. The MILP model in this work has approximately 1.5×10^5 continuous variables and 1.1×10^5 integer variables, which may take 15-40 minutes of computing time with an optimality gap of lower than 1%. The Gurobi commercial solver is applied to solve the co-optimization model, which is widely adopted to solve MILP problems with proven robustness and efficiency [41]. The branch-and-cut algorithm, embedded in Gurobi [36], makes it efficient for solving various integer programming problems with guaranteed optimality [42]. The description and flowchart of the branch-and-cut algorithm are given in **Appendix C**, while Refs. [43] and [44] provide more details regarding this algorithm and its applications to optimization problems.

3. Case study

A real-world case study was conducted in a multifunctional district in Shanghai, China. The selected district has 18 residential buildings, two shopping malls, one hotel, and two office buildings in which the energy station is built underground. The total floorage of the district is 128,500 m^2, including 51,700 m^2 residential buildings, 25,500 m^2 shopping malls, 32,000 m^2 hotels, and 19,300 m^2 office buildings. The layout of each building is shown in Fig. 5(a). The IES and layout of the heating and cooling networks are shown in Fig. 5(b). The 3D models of the buildings are shown in Fig. 5(c).
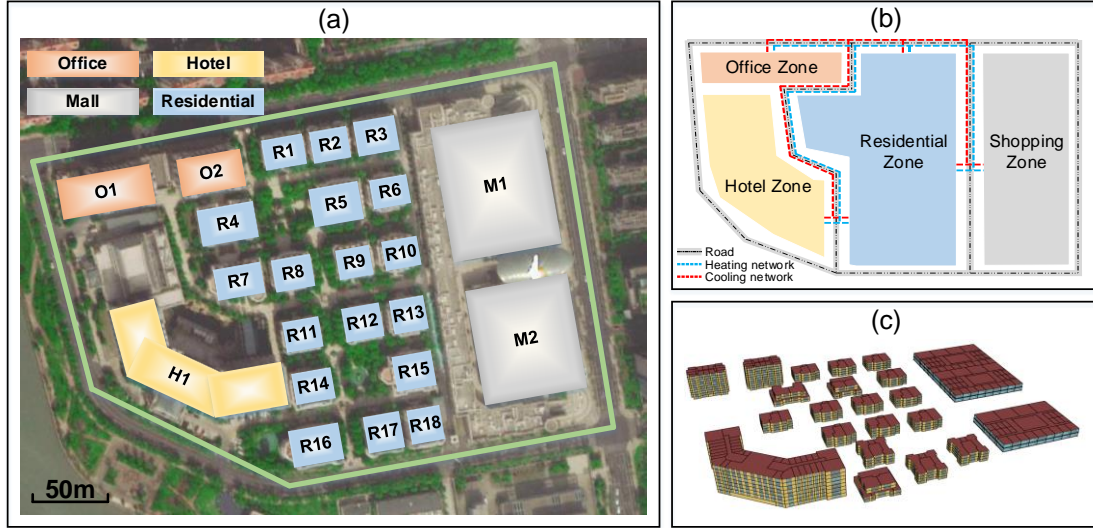
Fig. 5. Birds-eye view of the district with four categories of buildings (a), all buildings clustered into four functional zones and cooling/heating network layout (b), 3D model of the district (c).

3.1 Demand-side energy-saving effect quantification

Each demand-side scenario denotes a combination of external walls, roofs, and window upgrades. The scenario without implementing any upgrades is numbered as No. 1, and scenario No. 64 represents implementing the *Premium* upgrading of external walls, roofs, and windows. Fig. 6(a) presents the normalized annual energy demands of each demand-side scenario. It is evident that the annual cooling and heating demands would decrease further when implementing higher levels of upgrading on external walls, roofs, and windows. Meanwhile, the savings in annual cooling and heating demand could reach 20% and 30%, respectively. The upgrades of windows and roofs contribute to the more energy-saving effect of cooling demands, while the upgrades of the roof and external wall have a greater impact on heating demands. Fig. 6(b) illustrates the hourly electrical, cooling, and heating demands for one scenario. Detailed values of energy savings for each demand-side scenario are given in **Appendix B**.
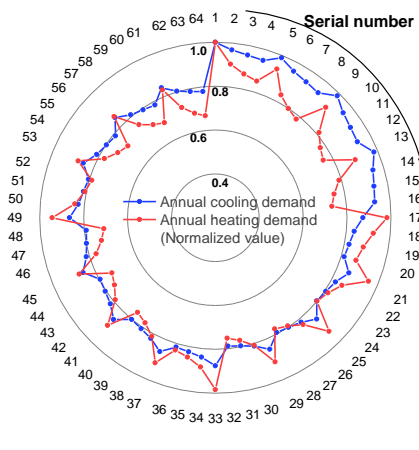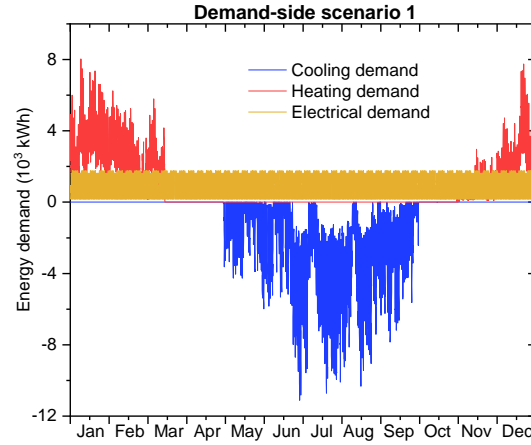
(a)   (b)

Fig. 6. Radar plot of cooling and heating saving effect when implementing 64 demand-side scenarios individually (a), illustrative hourly electrical, cooling and heating demands for scenario No. 1 (b).

3.2 Supply-side techno-economic parameterization

The supply-side module is parameterized by state-of-the-art inputs based on a conservative estimation of the technology lifetime of 15 years [45], and an assumed interest rate οf 6% [46]. The carbon emission factors of natural gas and bulk grid are set as 0.18 kg/kWh and 0.77 kg/kWh based on the East China grid's power supply. Other technical and economic parameters for supply-side technologies are listed in Table 3. The carbon tax in China is set within 0-70 \$/ton with a 10 \$/ton interval [47].

Table 3 Supply-side technical and economic parameters of the IES model. [16][34][48]

Technologies	Technical parameters		Economic parameters	
CHP	Power efficiency	0.42	Capital cost	1,200 \$/kW
	Heating efficiency	0.45	Maintenance cost	0.005 \$/kWh
	Maximum capacity	5,000 kW_e		
Gas boiler	Efficiency	0.85	Capital cost	80 \$/kW
	Maximum capacity	6,000 kW_h	Maintenance cost	0.0003 \$/kWh
Absorption chiller	Efficiency	0.9	Capital cost	180 \$/kW
	Maximum capacity	6,000 kW_c	Maintenance cost	0.002 \$/kWh
Electrical chiller	COP	4	Capital cost	120 \$/kW
	Maximum capacity	9,000 kW_c	Maintenance cost	0.002 \$/kWh
Heat pump	COP (Winter)	1.81	Capital cost	180 \$/kW
	COP (Others)	3	Maintenance cost	0.002 \$/kWh

	Maximum capacity	5,000 kW$_h$		
PV panels	Efficiency	0.15	Capital cost	1,650 \$/kW
	Total roof area	31,600 m^2	Maintenance cost	0.002 \$/kWh
Heat storage	Stored efficiency	0.9	Capital cost	75 \$/kW
	Charge efficiency	0.9	Maintenance cost	0.001 \$/kWh
	Discharge efficiency	0.9		
	Maximum capacity	5,000 kW$_h$		

4. Results and discussions

This section discusses the obtained results from four aspects: the economic benefit of co-optimization, impacts of the carbon tax on the optimal solution for demand and supply-sides, and uncertainty analysis results.

4.1 Economic benefit of co-optimization

Taking the supply-side-only optimization of IES as the baseline condition, the proposed co-optimization model could achieve more cost-efficient solutions, as shown by the cost breakdown in Fig. 7. The computational time of supply-side-only optimization model range from 5-10 minutes for one optimization, which is much lower than that of the co-optimization model. Meanwhile, with the increase of carbon level, the computational time of co-optimization model increases and reaches approximately 40 minutes when the carbon tax is 70 \$/ton. The lowest carbon tax (0 \$/ton) contributes to the least computational time of 15 minutes for the co-optimization model.

When the carbon tax is not considered, co-optimization and supply-side-only optimization achieve the same TACs as no demand-side upgrading is implemented. Once the carbon tax reaches 10 \$/ton, the optimal solutions of the co-optimization are better than those of the baseline model, and the differences increase with a higher carbon tax. The maximum difference is approximately 2.5% when the carbon tax is 70 \$/ton. This is because the co-optimization model significantly modified the structure of TAC by spending more on demand-side upgrading, leading to lower operation costs and carbon tax costs. Hence, the carbon tax, considered as the bridge, significantly influences the equilibrium between supply and demand-side decisions, while the optimal solutions show that the more carbon tax level contributes to the better

equilibrium.

When using the co-optimization model, the CAPEX values are generally higher than those of the baseline model because of the increasing capacity of renewable technologies. The OPEX values are reduced by 6 %–20% by introducing demand-side upgrading technologies, whereas additional cost of installation and replacement (i.e., UPEX) is required. Similarly, the energy-saving effect of co-optimization contributes to a 5%–15% reduction in CEEX. Generally, the increments of CAPEX and UPEX can be completely covered by the decrease in OPEX and CEEX in the co-optimization model, and economic benefits can be achieved.
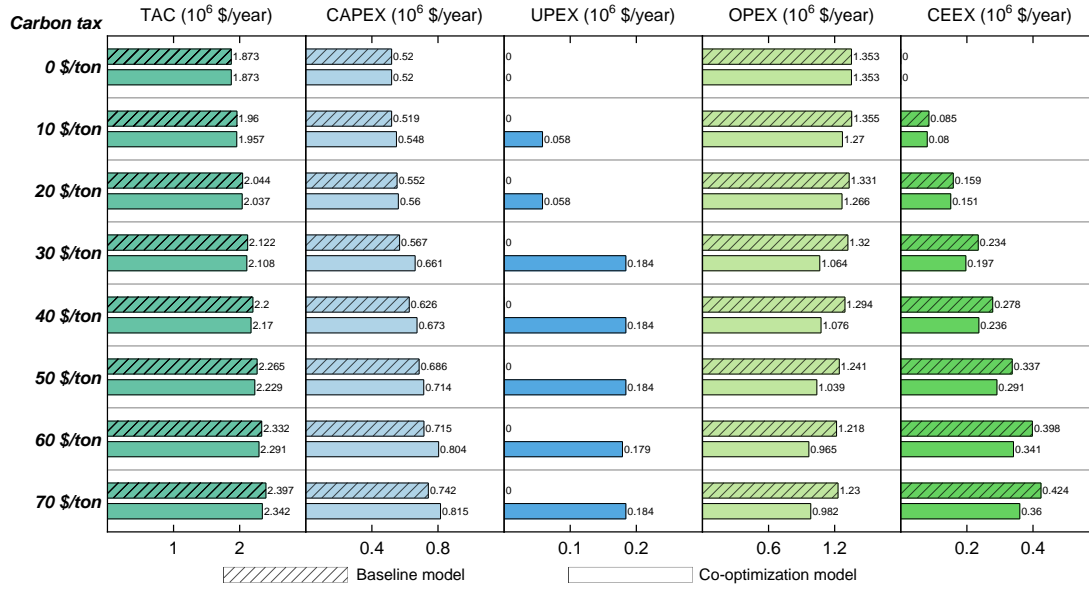
Fig. 7. Cost comparison between baseline model and co-optimization models considering various carbon tax. Abbreviation: TAC - total annual cost, CAPEX - capital cost, UPEX – upgrading cost, OPEX – operation cost, and CEEX – carbon tax.

The impacts of carbon tax on the TACs are further revealed in Fig. 8. For each carbon tax interval, OPEX is always the largest contributor, accounting for 72% to 42%. It also declines rapidly with the increase in carbon tax, corresponding decreased usage of fossil fuels, and the increasingly significant energy-saving effect. CAPEX ranged from 28% to 35%. Although several energy-supply technology capacities are reduced to some extent due to the demand-side upgrades, they cannot offset the significant increase in installing PV panels. Furthermore, the increasing carbon tax leads to an increase in the carbon tax cost (up to 8%), envelope upgrading cost (up to 15%), and

capital cost, while these additional costs can be fully covered by significant drops in operation costs.
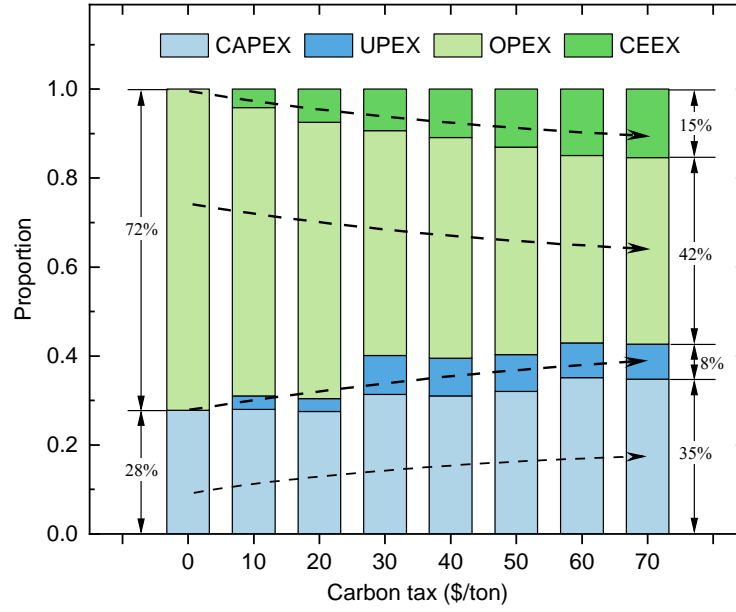
Fig. 8. Co-optimization models' cost breakdown considering various carbon tax. Abbreviation: TAC - total annual cost, CAPEX - capital cost, UPEX – upgrading cost, OPEX – operation cost, and CEEX – carbon tax.

4.2 Impacts of carbon tax on demand-side scheme

Table 4 indicates that a higher carbon tax would lead to the implementation of more improved envelope upgrading technologies to achieve more energy-saving effects. Without considering the carbon tax, none of the envelope upgrading technologies is selected so that the supply-side optimization and co-optimization obtain an identical result. Once the carbon tax is larger than zero, *Basic* roof upgrading would be immediately implemented. The *Basic* roof upgrading scheme is stable regardless of the carbon tax due to the higher upgrading cost of more improved alternatives. Meanwhile, the optimal demand-side scheme tends to select the *Basic* and *Standard* levels for the upgrades of windows and external walls. The *Premium* level for any envelope upgrading technology is not selected because of its huge investment expense. The maximum energy-saving amounts of cooling and heating demands could both reach 18.6%, and the more improved upgrading levels were not cost-efficient. In addition, the windows' upgrades usually account for the greatest proportion of upgrading costs, followed by roof and external wall upgrades. Note that this observation could be case-

specific, depending on the building shape, window-wall ratio, and material prices.

Table 4 Optimal demand-side scheme with cost breakdown and energy-saving effect.

Carbon tax ($/ton)	Upgrading scheme			Upgrading cost breakdown			Energy-saving effect	
	Window	Extwall*	Roof	Window	Extwall*	Roof	Cooling	Heating
0	*None*	*None*	*None*	0	0	0	0	0
10	*None*	*None*	*Basic*	0	0	100%	3.2%	9.7%
20	*None*	*None*	*Basic*	0	0	100%	3.2%	9.7%
30	*Standard*	*Basic*	*Basic*	44.2%	23.9%	31.9%	17.6%	18.6%
40	*Standard*	*Basic*	*Basic*	44.2%	23.9%	31.9%	17.6%	18.6%
50	*Standard*	*Basic*	*Basic*	44.2%	23.9%	31.9%	17.6%	18.6%
60	*Basic*	*Standard*	*Basic*	35.1%	32.2%	32.7%	18.4%	16.9%
70	*Standard*	*Basic*	*Basic*	44.2%	23.9%	31.9%	17.6%	18.6%

*Extwall is the external wall

4.3 Impacts of carbon tax on supply-side design

The overall system performance and supply-side design are significantly affected by the carbon tax, as discussed in the following subsections.

4.3.1 Energy carrier shares

Fig. 9 shows the entire system's energy carrier shares of natural gas use, electricity from the bulk grid, and renewable resources. In general, carbon taxes increase renewable power generation and reduce onsite natural gas usage. The bulk grid shares are relatively steady to ensure system reliability. The dots representing the supply-side scenarios of the transition seasons are distributed on the renewable axis due to no heating and cooling demands, while the electrical demands are fulfilled by PV panels and the bulk grid (CHP is off). With the increase in carbon tax, the renewable share increases significantly, with a maximum value of up to 58%. Meanwhile, because the emission factor of the bulk power grid is much higher than that in Europe [15] and subsidies on CHP in China, low-cost natural gas would be increasingly utilized to generate onsite power. Consequently, the dots representing winter and summer supply-side scenarios are distributed around the bottom-right region with natural gas shares of more than 50% and bulk grid shares of less than 25%. With the increase in carbon tax, the natural gas share decreased from 85% to 57%, while the bulk grid share reduced significantly from 14% to 6%. In addition, a comparison between Fig. 9(a) and Fig. 9(b)

reveals that the higher carbon tax intervals push the distribution's region toward lower natural gas shares and higher renewable shares more powerfully than the lower carbon tax intervals, and then obtain more disperse distributions, meaning diversified combinations of energy carrier shares. Furthermore, the energy carrier shares are closely related to the system configurations and dispatch strategy, as reported in the following subsections.
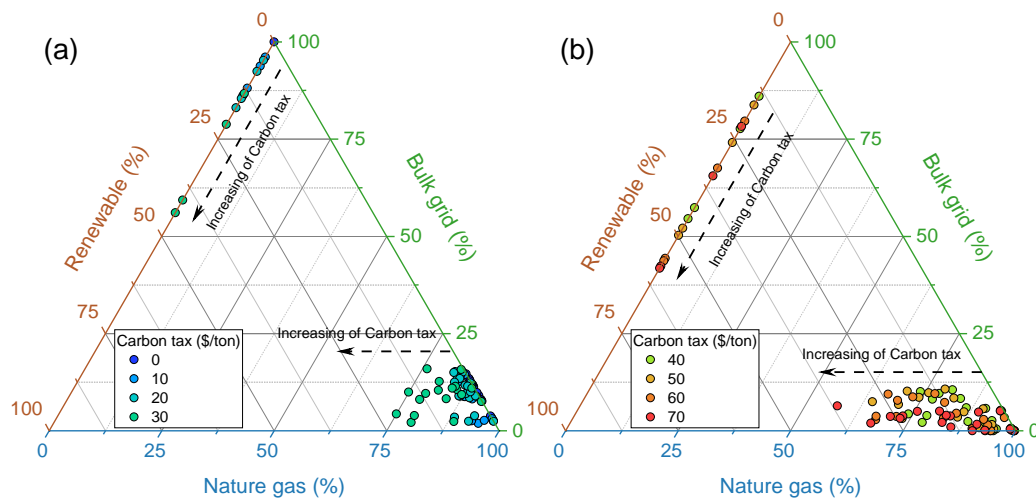
Fig. 9. Energy carrier shares' variations with carbon tax, 0-30 $/ton (a) and 40-70 $/ton (b). The energy carrier shares for each supply-side scenario are shown as a series of dots with various colors for representing corresponding carbon tax.

4.3.2 Capacity configuration

Fig. 10 presents the optimal supply-side designs with eight carbon tax intervals. Generally, the carbon tax boosts the supply-side design and demand-side scheme towards a more renewable and energy-saving manner. PV panels were not installed when the carbon tax was zero. With the increase in carbon tax from 10 to 30 $/ton, the installed capacity of PV panels increases gradually, and its installed area increases from 2,692 m^2 to 9,212 m^2, which is equivalent to approximately 10% to 30% of the overall available roofs. Hence, this carbon tax can be considered as the reference value to decide upon the massive introduction of renewable energy technologies in district-level IES with an economic objective. Although the carbon tax reaches the upper bound of 70 $/ton, the proportion of the total area of PV-installed roofs to that of all roofs is no more than 50% (15,800 m^2) due to the higher cost of installation and maintenance when compared to other fuel-based technologies. As various envelope upgrading schemes are

adopted on the demand side, the increasing carbon tax lowers the installed capacities of the natural gas-based technologies - that is, the capacities of CHP, HP, and AC reduce by more than 20%, while the capacities of Boiler and EC are reduced by approximately 15% and 18%, respectively. Interestingly, the capacity of HS initially decreases and then increases as a larger capacity of heat storage could contribute to lower carbon emissions during the operation stage.
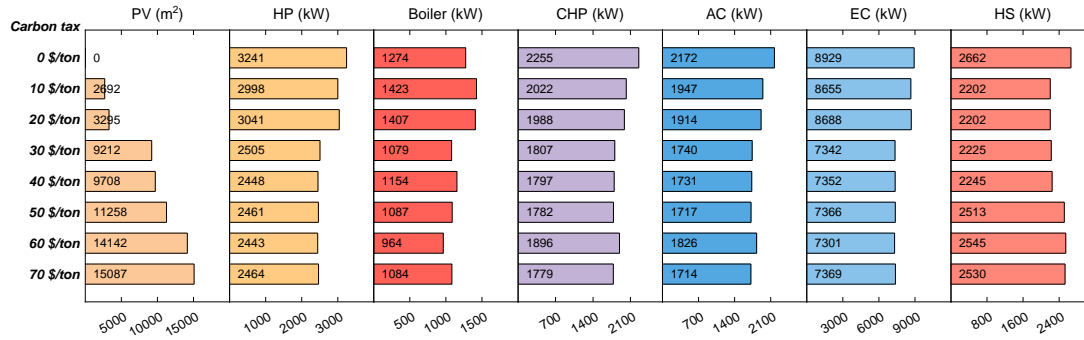
Fig. 10. Optimal supply-side design of capacity configuration with various levels of carbon tax.

4.3.3 Dispatch strategy

The hourly cooling and heating balances for the two representative supply-side scenarios with the highest probabilities are shown in Fig. 11.

Summer cooling balances for 0 $/ton and 70 $/ton carbon taxes are illustrated in Fig. 11(a-d). When the carbon tax is not charged, the absorption chiller provides more cooling energy than the electrical chiller, along with a larger capacity of CHP and available heating. However, the opposite is true for the 70 $/ton carbon tax – the majority of electricity consumed by the electrical chiller is fed from renewable rather than CHP or bulk grid, which is in line with observations for the energy carrier shares. Because the fluctuation of cooling demand is coincident with the variation of the peak-valley electricity price, the impact of TOU price on optimal dispatch strategies for summer is insignificant in this case.

Figure 11(e-h) illustrates the heating balances of several representative supply-side scenarios during winter. There is an obvious difference in the scheduling of CHP between the 0 $/ton carbon tax and 70 $/ton carbon tax. When the carbon tax is 0 $/ton, CHP tends to be shut down during the valley period of the TOU electricity price. However, CHP operates all the time when the carbon tax is 70 $/ton. This is because

the optimal solution with a high carbon tax would have to choose the CHP-generated electricity instead of the bulk grid electricity with a high emission factor, even if the bulk grid electricity price is lower. Similarly, the heat pump tends to provide more heating when the carbon tax is 0 $/ton. Meanwhile, heat storage can provide flexibility in the scheduling of heating balances.

The hourly electrical balances of the scenarios with the highest probabilities in each season considering 0 $/ton and 70 $/ton carbon tax are shown in Fig. 12(a) and (d) for summer, Fig. 12(b) and (e) for winter, and Fig. 12(c) and (f) for the transition seasons, respectively. In general, the optimal dispatch strategy is comprehensively affected by the energy carrier prices, technical parameters, carbon emission factors, upgrading prices, and carbon tax. Unlike the heating and cooling balances, there is no difference in the electrical demand between the low and high carbon taxes, while their optimal dispatch strategies vary greatly. For the 0 $/ton carbon tax, the CHP is usually in full-load operation and feeds a relatively greater amount of surplus electricity back to the grid during the daytime peak. Meanwhile, the PV panels play a more important role when the carbon tax is 70 $/ton.
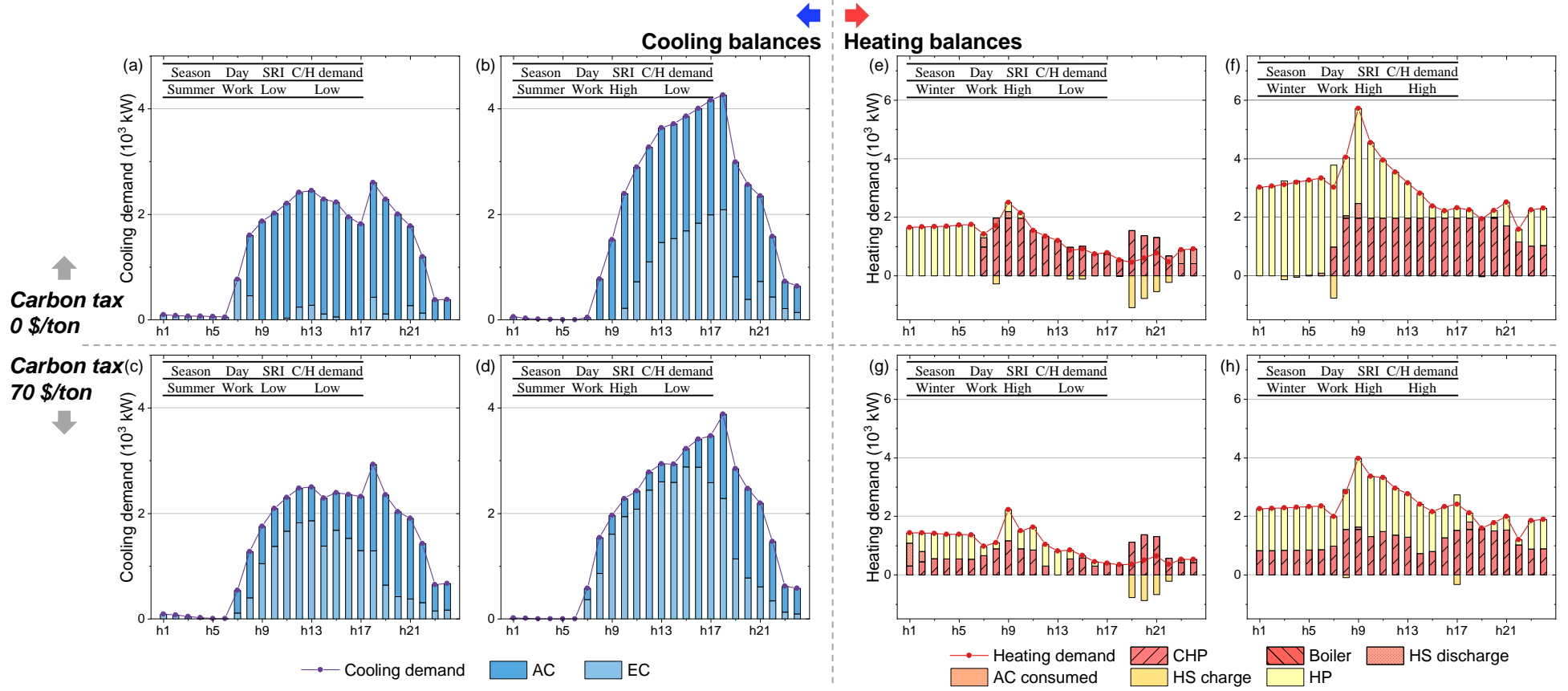
Fig. 11. Representative supply-side scenarios' cooling balances for scenarios 1 and 3, and heating balances for scenarios 11 and 12, with the carbon tax of 0 $/ton (a-d) and 70 $/ton (e-h).

Fig. 12. Representative supply-side scenarios' electrical balances of scenarios 3, 11, and 17 for 0 $/ton carbon tax (a-c), and for 70 $/ton carbon tax (d-f).

4.4 Uncertainty analysis results

Uncertainties exist from parameter assumptions, and this work investigates the uncertainty of the most influential uncertain factor, prices, by combining Monte Carlo simulation with optimization of the operation variables only while fixing the design variables. The number of simulations was set to 5000. Owing to the computational resource limits, the uncertainty analysis was performed on the optimal results of five representative values of carbon tax, as shown by the violin plot in Fig. 13 and reported in Table 5.
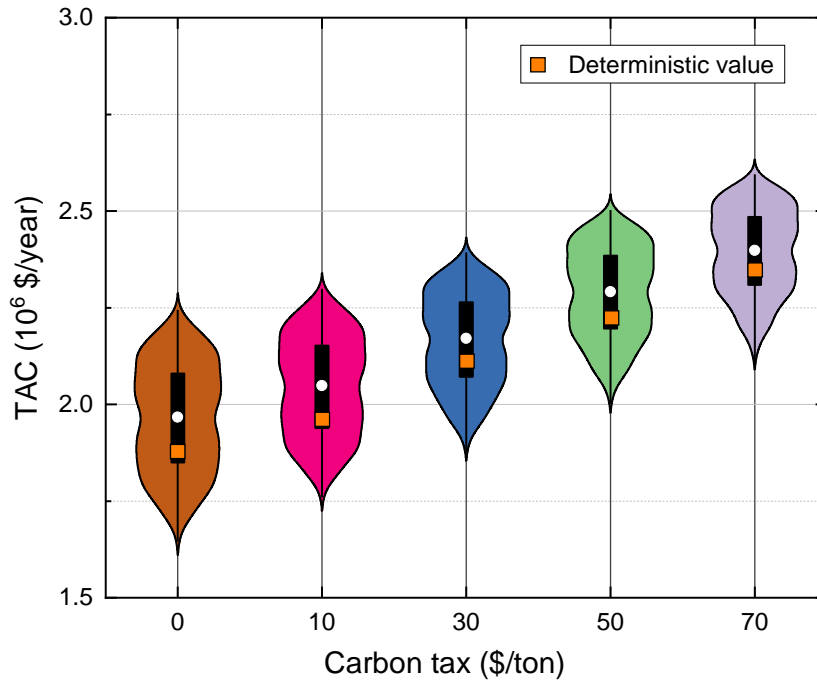
Fig. 13. Violin plot of TAC distributions obtained by uncertainty analysis in terms of various carbon tax.

As shown in Fig. 13, each violin plot demonstrates the robustness of the optimal designs for the demand and supply-sides under the uncertainties of prices. The box indicates the range of the lower quartile to the upper quartile, the white dot represents the distribution's mean value, and the whisker shows the range of the 5th percentile to the 95th percentile. The coefficient of variation (CV), standard deviation (STD), and mean value are listed in Table 5 for quantification purposes, and the deterministic values discussed in Section 4.1. The CV indicator characterizes the dispersion degree of distributions, which is defined as the ratio of the STD to the mean value. Intuitively, the mean values are slightly greater than the deterministic values, indicating that the

optimal performance deteriorates with the introduction of uncertainties. With an increase in the carbon tax, the deviations gradually decrease because of a higher proportion of carbon emission cost, whose relative value ranges from 5% to 2%. Consequently, the CV value varies from 6.9% to 4.5%, which means that the distribution becomes more concentrated with a higher carbon tax. In general, the robustness of the proposed co-optimization model was validated by uncertainty analysis. The optimal demand-side scheme and supply-side capacity configuration are capable of addressing the uncertainties from prices at the operation stage, including the ratio of replacement and maintenance costs of envelopes (i.e., window, external wall, and roof), the energy carrier prices (i.e., natural gas and bulk grid), and the ratio of the FIT to purchased price from the bulk grid.

Table 5 Mean and standard deviation of TAC for various carbon tax

System performance	Carbon tax ($/ton)	Deterministic (10^6 \$/year)	Mean (10^6 \$/year)	STD (10^6 \$/year)	CV (%)
	0	1.873	1.964	0.137	6.98
	10	1.958	2.045	0.126	6.19
TAC	30	2.109	2.165	0.117	5.42
	50	2.229	2.287	0.115	5.01
	70	2.343	2.393	0.108	4.52

4.5 Model scalability and adoptability

The proposed co-optimization model is featured by scalability and adoptability. The designers can flexibly modify the supply and demand-side scenario trees according to their specific needs and computational resources. The model adoptability is reflected by covering the typical energy technologies widely used in IES system. The co-optimization modeling concept could be adapted to other districts in various climate zones and scaled to large-scale case studies such as urban areas including dozens of multi-functional buildings. In addition, the proposed study unlocked the impacts of carbon tax on IES from a whole-system decision-maker perspective and is expected to benefit the supply and demand-side stakeholders to achieve a low-carbon and economic design. Beyond the district studied in present work, the proposed co-optimization model could be implemented in other countries or climate zones by considering the

local technical-economic-environmental characteristics and renewable resources.

5. Conclusions

To unlock the impacts of the emerging carbon tax on integrated energy systems (IES), this study develops an IES co-optimization model incorporating supply-side and demand-side energy technologies. A selection tree and a binary tree were introduced to represent various demand-side and supply-side scenarios, respectively. The demand-side module considers four envelope upgrading levels (i.e., *None*, *Basic*, *Standard*, and *Premium*) for external walls, roofs, and windows, respectively, and the EnergyPlus building energy simulation tool is adopted to explicitly quantify the saving effects. The supply-side module consists of various supply-side scenarios using clustering-based methods that describe the variations from seasons, occupant behaviors, and renewable resources. The two modules are integrated into an improved stochastic programming model to capture the impact of the carbon tax. Furthermore, an uncertainty analysis combining Monte Carlo simulation and operation optimization was conducted to validate the robustness of the proposed co-optimization model when considering price uncertainties at the operation stage. The major conclusions are summarized as follows:

(1) The case study at a multifunctional district in Shanghai, China, reveals that the co-optimization model can achieve a 2.5% more cost-efficient IES design than the supply-side-only optimization model when up to 70 \$/ton of carbon tax is considered.

(2) Carbon tax will promote the implementation of demand-side upgrading schemes. The *Basic* upgrading for roofs and external walls and the *Standard* upgrading for windows are preferred, while the *Premium* is not cost-efficient even when the carbon tax is up to 70 \$/ton.

(3) Introducing the carbon tax leads to a capacity drop of 15–24% for fuel-based technologies and a significant increase in the installed area of PV panels. A relatively steady share of the bulk grid is observed, which can contribute to system reliability.

(4) The uncertainty analysis validates the robustness of the optimal solutions considering the uncertainties of various prices. The relative difference between deterministic values and mean values is less than 5%, and the distributions are

concentrated acceptably with CV values of no more than 7%.

In general, this study unlocks the emerging impacts of carbon tax on IES by proposing a supply and demand co-optimization model. The optimal results were validated against the uncertainties. The observations could inform the future design of IES and assist in preparation for the forthcoming carbon tax. This work can be extending in the future by introducing more demand-side energy-saving technologies, e.g., demand response and EV charging, and adopting advanced supply-side modeling methods, including multi-energy hub approach and intelligence-based techniques. Meanwhile, a multi-objective optimization approach can also be considered to achieve Pareto optimality so that the energy planning model provides more optimal alternatives for stakeholders and decision-makers.

Declaration of interest

There are no conflicts of interests to declare.

References

[1]   Klemm C, Vennemann P. Modeling and optimization of multi-energy systems in mixed-use districts: A review of existing methods and approaches. Renew Sustain Energy Rev 2021;135:110206. https://doi.org/10.1016/j.rser.2020.110206.

[2]   EUROPEAN COMMISSION. Powering a climate-neutral economy: An EU Strategy for Energy System Integration. 2020.

[3]   Ridha E, Nolting L, Praktiknjo A. Complexity profiles: A large-scale review of energy system models in terms of complexity. Energy Strateg Rev 2020;30:100515. https://doi.org/10.1016/j.esr.2020.100515.

[4]   Twaha S, Ramli MAM. A review of optimization approaches for hybrid distributed energy generation systems: Off-grid and grid-connected systems. Sustain Cities Soc 2018;41:320–31. https://doi.org/10.1016/j.scs.2018.05.027.

[5]   Siddaiah R, Saini RP. A review on planning, configurations, modeling and optimization techniques of hybrid renewable energy systems for off grid applications. Renew Sustain Energy Rev 2016;58:376–96. https://doi.org/10.1016/j.rser.2015.12.281.

[6]   Jing R, Wang M, Wang W, Brandon N, Li N, Chen J, et al. Economic and environmental multi-optimal design and dispatch of solid oxide fuel cell based CCHP system. Energy Convers Manag 2017;154:365–79. https://doi.org/10.1016/j.enconman.2017.11.035.

[7]   Wang Y, Ma Y, Song F, Ma Y, Qi C, Huang F, et al. Economic and efficient multi-objective operation optimization of integrated energy system considering electro-thermal demand response. Energy 2020;205:118022. https://doi.org/10.1016/j.energy.2020.118022.

[8]   Mayer MJ, Szilágyi A, Gróf G. Environmental and economic multi-objective optimization of a household level hybrid renewable energy system by genetic algorithm. Appl Energy 2020;269:115058. https://doi.org/10.1016/j.apenergy.2020.115058.

[9]   Mu C, Ding T, Qu M, Zhou Q, Li F, Shahidehpour M. Decentralized optimization operation for the multiple integrated energy systems with energy cascade utilization. Appl Energy 2020;280:115989. https://doi.org/10.1016/j.apenergy.2020.115989.

[10]   Wu D, Han Z, Liu Z, Li P, Ma F, Zhang H, et al. Comparative study of optimization method and optimal operation strategy for multi-scenario integrated energy system. Energy 2021;217. https://doi.org/10.1016/j.energy.2020.119311.

[11]   Kang L, Yang J, An Q, Deng S, Zhao J, Wang H, et al. Effects of load following operational strategy on CCHP system with an auxiliary ground source heat pump considering carbon tax and electricity feed in tariff. Appl Energy 2017;194:454–66. https://doi.org/10.1016/j.apenergy.2016.07.017.

[12]   Dorotić H, Pukšec T, Duić N. Analysis of displacing natural gas boiler units in district heating systems by using multi-objective optimization and different taxing approaches. Energy Convers Manag 2020;205. https://doi.org/10.1016/j.enconman.2019.112411.

[13]   Martelli E, Freschini M, Zatti M. Optimization of renewable energy subsidy and carbon tax for multi energy systems using bilevel programming. Appl Energy 2020;267:115089. https://doi.org/10.1016/j.apenergy.2020.115089.

[14]   Mavromatidis G, Orehounig K, Carmeliet J. Uncertainty and global sensitivity analysis for the optimal design of distributed energy systems. Appl Energy 2018;214:219–38. https://doi.org/10.1016/j.apenergy.2018.01.062.

[15]   Mavromatidis G, Orehounig K, Carmeliet J. Design of distributed energy systems under uncertainty: A two-stage stochastic programming approach. Appl Energy 2018;222:932–50. https://doi.org/10.1016/j.apenergy.2018.04.019.

[16]   Wang M, Yu H, Jing R, Liu H, Chen P, Li C. Combined multi-objective optimization and robustness analysis framework for building integrated energy system under uncertainty. Energy Convers Manag 2020;208:112589. https://doi.org/10.1016/j.enconman.2020.112589.

[17]   Diakaki C, Grigoroudis E, Kolokotsa D. Performance study of a multi-objective mathematical programming modelling approach for energy decision-making in buildings. Energy 2013;59:534–42. https://doi.org/10.1016/j.energy.2013.07.034.

[18]   Chen Y, Xu P, Chen Z, Wang H, Sha H, Ji Y, et al. Experimental investigation of demand response potential of buildings: Combined passive thermal mass and active storage. Appl Energy 2020;280:115956. https://doi.org/10.1016/j.apenergy.2020.115956.

[19]   Liu Y, Liu T, Ye S, Liu Y. Cost-benefit analysis for Energy Efficiency Retrofit of existing buildings: A case study in China. J Clean Prod 2018;177:493–506. https://doi.org/10.1016/j.jclepro.2017.12.225.

[20]   Wang Y, Wei C. Design optimization of office building envelope based on quantum genetic algorithm for energy conservation. J Build Eng 2021;35:102048. https://doi.org/10.1016/j.jobe.2020.102048.

[21]   Chang S, Castro-Lacouture D, Yamagata Y. Decision support for retrofitting building envelopes using multi-objective optimization under uncertainties. J Build Eng 2020;32:101413. https://doi.org/10.1016/j.jobe.2020.101413.

[22]   Zheng X, Qiu Y, Zhan X, Zhu X, Keirstead J, Shah N, et al. Optimization based planning of urban energy systems: Retrofitting a Chinese industrial park as a case-study. Energy 2017;139:31–41. https://doi.org/10.1016/j.energy.2017.07.139.

[23]   Ferrara M, Rolfo A, Prunotto F, Fabrizio E. EDeSSOpt – Energy Demand and Supply Simultaneous Optimization for cost-optimized design: Application to a multi-family building. Appl Energy 2019;236:1231–48. https://doi.org/10.1016/j.apenergy.2018.12.043.

[24]   Perera ATD, Javanroodi K, Nik VM. Climate resilient interconnected infrastructure: Co-optimization of energy systems and urban morphology. Appl Energy 2021;285:116430. https://doi.org/10.1016/j.apenergy.2020.116430.

[25]   Liu Z, Yu H, Liu R. A novel energy supply and demand matching model in park integrated energy system. Energy 2019;176:1007–19. https://doi.org/10.1016/j.energy.2019.04.049.

[26]   Shanghai Municipal Commission of Housing and Urban Rural Development. Design standard for energy efficiency of residential buildings 2015:DGJ08-205–2015.

[27]   Yan D, Hong T, Li C, Zhang Q, An J, Hu S. A thorough assessment of China's standard for energy consumption of buildings. Energy Build 2017;143:114–28. https://doi.org/10.1016/j.enbuild.2017.03.019.

[28]   Jing R, Kuriyan K, Lin J, Shah N, Zhao Y. Quantifying the contribution of individual technologies in integrated urban energy systems – A system value approach. Appl Energy 2020;266:114859. https://doi.org/10.1016/j.apenergy.2020.114859.

[29]   Zhang X. Life Cycle Economic Analysis of NZEB Technical Strategies for Office Building in Yangtze River Delta. Southeast University, 2019.

[30]   Yu J, Tian L, Xu X, Wang J. Evaluation on energy and thermal performance for office building envelope in different climate zones of China. Energy Build 2015;86:626–39.

https://doi.org/10.1016/j.enbuild.2014.10.057.

[31] Song X, Ye C, Li H, Wang X, Ma W. Field study on energy economic assessment of office buildings envelope retrofitting in southern China. Sustain Cities Soc 2017;28:154–61. https://doi.org/10.1016/j.scs.2016.08.029.

[32] Thalfeldt M, Pikas E, Kurnitski J, Voll H. Window model and 5 year price data sensitivity to cost-effective façade solutions for office buildings in Estonia. Energy 2017;135:685–97. https://doi.org/10.1016/j.energy.2017.06.160.

[33] Ruiz LGB, Pegalajar MC, Arcucci R, Molina-Solana M. A time-series clustering methodology for knowledge extraction in energy consumption data. Expert Syst Appl 2020;160:113731. https://doi.org/10.1016/j.eswa.2020.113731.

[34] Wang M, Yu H, Lin X, Jing R, He F, Li C. Comparing stochastic programming with posteriori approach for multi-objective optimization of distributed energy systems under uncertainty. Energy 2020;210:118571. https://doi.org/10.1016/j.energy.2020.118571.

[35] Zheng Z, Li X, Pan J, Luo X. A multi-year two-stage stochastic programming model for optimal design and operation of residential photovoltaic-battery systems. Energy Build 2021;239:110835. https://doi.org/10.1016/j.enbuild.2021.110835.

[36] Schütz T, Schiffer L, Harb H, Fuchs M, Müller D. Optimal design of energy conversion units and envelopes for residential building retrofits using a comprehensive MILP model. Appl Energy 2017;185:1–15. https://doi.org/10.1016/j.apenergy.2016.10.049.

[37] Bahlawan H, Morini M, Pinelli M, Poganietz WR, Spina PR, Venturini M. Optimization of a hybrid energy plant by integrating the cumulative energy demand. Appl Energy 2019;253:113484. https://doi.org/10.1016/j.apenergy.2019.113484.

[38] Moslehi S, Reddy TA. An LCA methodology to assess location-specific environmental externalities of integrated energy systems. Sustain Cities Soc 2019;46:101425. https://doi.org/10.1016/j.scs.2019.101425.

[39] Zhang C, Xue X, Du Q, Luo Y, Gang W. Study on the performance of distributed energy systems based on historical loads considering parameter uncertainties for decision making. Energy 2019;176:778–91. https://doi.org/10.1016/j.energy.2019.04.042.

[40] Dimov I, Georgieva R. Monte Carlo algorithms for evaluating Sobol' sensitivity indices. Math Comput Simul 2010;81:506–14. https://doi.org/10.1016/j.matcom.2009.09.005.

[41] Jing R, Li Y, Wang M, Chachuat B, Lin J, Guo M. Coupling biogeochemical simulation and mathematical optimisation towards eco-industrial energy systems design. Appl Energy 2021;290:116773. https://doi.org/10.1016/j.apenergy.2021.116773.

[42] Naud O, Tisseyre B. Branch and Cut Support to decision-making 21st European Symposium on Comput- er Aided Process Engineering Application of Optimization Tech- niques for Protection and Restoration Design 11th International Symposium on Process Systems Engineering 27th Europ 2020:2015–8.

[43] Wolfinger D, Salazar-González JJ. The Pickup and Delivery Problem with Split Loads and Transshipments: A Branch-and-Cut Solution Approach. Eur J Oper Res 2021;289:470–84. https://doi.org/10.1016/j.ejor.2020.07.032.

[44] Heßler K, Irnich S. A branch-and-cut algorithm for the soft-clustered vehicle-routing problem. Discret Appl Math 2021;288:218–34. https://doi.org/10.1016/j.dam.2020.08.017.

[45] Zhang Z, Jing R, Lin J, Wang X, van Dam KH, Wang M, et al. Combining agent-based residential demand modeling with design optimization for integrated energy systems planning

and operation. Appl Energy 2020;263:114623. https://doi.org/10.1016/j.apenergy.2020.114623.

[46]   Jing R, Wang M, Liang H, Wang X, Li N, Shah N, et al. Multi-objective optimization of a neighborhood-level urban energy network: Considering Game-theory inspired multi-benefit allocation constraints. Appl Energy 2018;231:534–48. https://doi.org/10.1016/j.apenergy.2018.09.151.

[47]   An Y, Zhai X. SVR-DEA model of carbon tax pricing for China's thermal power industry. Sci Total Environ 2020;734:139438. https://doi.org/10.1016/j.scitotenv.2020.139438.

[48]   Jing R, Wang M, Zhang Z, Wang X, Li N, Shah N, et al. Distributed or centralized? Designing district-level urban energy systems by a hierarchical approach considering demand uncertainties. Appl Energy 2019;252:113424. https://doi.org/10.1016/j.apenergy.2019.113424.

[49]   P Kumar P, Saini RP. Optimization of an off-grid integrated hybrid renewable energy system with various energy storage technologies using different dispatch strategies. Energy Sources, Part A Recover Util Environ Eff 2020:1–30. https://doi.org/10.1080/15567036.2020.1824035.

[50]   Maleki A. Design and optimization of autonomous solar-wind-reverse osmosis desalination systems coupling battery and hydrogen energy storage by an improved bee algorithm. Desalination 2018;435:221–34. https://doi.org/10.1016/j.desal.2017.05.034.

[51]   Kumar PP, Saini RP. Optimization of an off-grid integrated hybrid renewable energy system with different battery technologies for rural electrification in India. J Energy Storage 2020;32:101912. https://doi.org/10.1016/j.est.2020.101912.

[52]   Patel AM, Singal SK. Optimal component selection of integrated renewable energy system for power generation in stand-alone applications. Energy 2019;175:481–504. https://doi.org/10.1016/j.energy.2019.03.055.

[53]   Lee S, Kim H, Kim TH, Shin H, Kim W. Fault current constraint transmission expansion planning based on the inverse matrix modification lemma and a valid inequality. Energies 2019;12. https://doi.org/10.3390/en12244769.

Appendix A

The model's mathematical constraints of each component are developed based on previous research and presented below.

A.1 Capacity constraints

An upper bound must exist, which provides the maximum installed capacity for each energy conversion technology, while the total roof area of buildings limits the maximum capacity of PV panels [49].

$$CAP_k \leq CAP_k^{\max} \tag{A1a}$$

$$AREA_{\mathrm{pv}} \leq AREA^{\mathrm{roof}} \tag{A1b}$$

Considering the complexity of the proposed co-optimization model, constant efficiency is used to describe the performance of each energy conversion technology to ensure the linearity of the model; the output of each technology cannot exceed its installed capacity.

$$Q_{\mathrm{chp},s,h}^{\mathrm{ele}} \leq CAP_{\mathrm{chp}} \tag{A2a}$$

$$Q_{\mathrm{b},s,h}^{\mathrm{heat}} \leq CAP_{\mathrm{b}} \tag{A2b}$$

$$Q_{\mathrm{hp},s,h}^{\mathrm{heat}} \leq CAP_{\mathrm{hp}} \tag{A2c}$$

$$Q_{\mathrm{hs},s,h}^{\mathrm{heat}} \leq CAP_{\mathrm{hs}} \tag{A2d}$$

$$Q_{\mathrm{ec},s,h}^{\mathrm{cool}} \leq CAP_{\mathrm{ec}} \tag{A2e}$$

$$Q_{\mathrm{ac},s,h}^{\mathrm{cool}} \leq CAP_{\mathrm{ac}} \tag{A2f}$$

where *CAP* indicates the installed capacity of the energy technologies.

A.2 Operation constraints

A.2.1 CHP

The CHP operation is constrained by Eq. (A3). This constraint set includes load-ratio constraints to avoid operation at a low load ratio in Eq. (A3c–A3d), the ramping constraint, which avoids drastic variations in Eq. (A3e), and the maximum startup constraint that avoids frequent start-ups in Eq. (A3f–A3i), such that its efficiency is stable and life can be extended [50].

$$Q_{\mathrm{chp},s,h}^{\mathrm{ele}} = \eta_{\mathrm{chp}}^{\mathrm{ele}} \times NG_{\mathrm{chp},s,h} \tag{A3a}$$

$$Q_{\mathrm{chp},s,h}^{\mathrm{heat}} = \eta_{\mathrm{chp}}^{\mathrm{heat}} \times NG_{\mathrm{chp},s,h} \tag{A3b}$$

$$Q_{\text{chp},s,h}^{\text{ele}} \leq \varphi_{\text{chp},s,h} \times CAP_{\text{chp}} \tag{A3c}$$

$$Q_{\text{chp},s,h}^{\text{ele}} \geq 0.2 \times \varphi_{\text{chp},s,h} \times CAP_{\text{chp}} \tag{A3d}$$

$$-0.5 \times CAP_{\text{chp}} \leq Q_{\text{chp},s,h+1}^{\text{ele}} - Q_{\text{chp},s,h}^{\text{ele}} \leq 0.5 \times CAP_{\text{chp}} \tag{A3e}$$

$$\sum_h \gamma_{\text{chp},s,h} \leq 1 \tag{A3f}$$

$$\gamma_{\text{chp},s,h} \geq \varphi_{\text{chp},s,h} - \varphi_{\text{chp},s,h-1} \tag{A3g}$$

$$\gamma_{\text{chp},s,h} \leq 1 - \varphi_{\text{chp},s,h-1} \tag{A3h}$$

$$\gamma_{\text{chp},s,h} \leq \varphi_{\text{chp},s,h} \tag{A3i}$$

where the binary variables φ and γ denote the on/off status and startup time, respectively.

A.2.2 Heat storage tank and grid interaction

The IES model also introduces a heat storage tank owing to its economic attractiveness and maturity, while off-grid IES systems cannot ensure robustness. The modules of heat storage and grid interaction both need to avoid inputting and outputting concurrently, and the binary variables φ are then introduced. For the heat storage module in Eq. (A4), the efficiencies of the intertemporal loss, charging, and discharging are introduced to describe the intertemporal balance [51].

$$Q_{\text{hs},s,h}^{\text{heat}} = \eta_{\text{hs}} \times Q_{\text{hs},s,h-1}^{\text{heat}} + \eta_{\text{hs-in}} \times Q_{\text{hs-in},s,h}^{\text{heat}} - \frac{Q_{\text{hs-out},s,h}^{\text{heat}}}{\eta_{\text{hs-out}}} \tag{A4a}$$

$$Q_{\text{hs-in},s,h}^{\text{heat}} \leq \varphi_{\text{hs-in},s,h} \times CAP_{\text{hs}} \tag{A4b}$$

$$Q_{\text{hs-out},s,h}^{\text{heat}} \leq \varphi_{\text{hs-out},s,h} \times CAP_{\text{hs}} \tag{A4c}$$

$$\varphi_{\text{hs-in},s,h} + \varphi_{\text{hs-out},s,h} \leq 1 \tag{A4d}$$

The expressions for grid interaction, including electricity purchasing and feedback, are listed in Eq. (A5).

$$0 \leq Q_{\text{im},s,h}^{\text{ele}} \leq \varphi_{\text{im},s,h} \times CAP_{\text{grid}} \tag{A5a}$$

$$0 \leq Q_{\text{ex},s,h}^{\text{ele}} \leq \varphi_{\text{ex},s,h} \times CAP_{\text{grid}} \tag{A5b}$$

$$\varphi_{\text{ex},s,h} + \varphi_{\text{im},s,h} \leq 1 \tag{A5c}$$

where CAP_{grid} is the maximum capacity of grid purchasing based on the on-grid agreement.

A.2.3 Other constraints

In addition to the above energy technologies with special operation constraints, the modules of electrical chillers, absorption chillers, gas boilers, air-source heat pumps, and PV panels have a linear relationship between their outputs and the energy or energy

carriers consumed, as shown in Eq. (A6). Note that the heat pumps have different efficiencies in summer and winter owing to the ambient temperature [52].

$$Q_{\text{ec},s,h}^{\text{cool}} = \eta_{\text{ec}} \times Q_{\text{ec},s,h}^{\text{ele}} \tag{A6a}$$

$$Q_{\text{hp},s,h}^{\text{heat}} = \eta_{\text{hp-win/hp-sum}} \times Q_{\text{hp},s,h}^{\text{ele}} \tag{A6b}$$

$$Q_{\text{ac},s,h}^{\text{cool}} = \eta_{\text{ac}} \times Q_{\text{ac},s,h}^{\text{heat}} \tag{A6c}$$

$$Q_{\text{b},s,h}^{\text{cool}} = \eta_{\text{b}} \times NG_{\text{b},s,h} \tag{A6d}$$

$$Q_{\text{pv},s,h}^{\text{ele}} = \eta_{\text{pv}} \times SRI_{s,h} \times AREA_{\text{pv}} \tag{A6e}$$

Appendix B

See Table B1.

Table B1 Energy demands and envelope upgrading scheme for each demand-side scenario

Scenario	Envelope upgrading scheme			Annual energy demand (10^6 kWh)		Scenario	Envelope upgrading scheme			Annual demand (10^6 kWh)	
	Window	Extwall	Roof	Cooling	Heating		Window	Extwall	Roof	Cooling	Heating
1	*None*	*None*	*None*	9.975	6.935	33	*Standard*	*None*	*None*	8.724	6.824
2	*None*	*None*	*Basic*	9.661	6.265	34	*Standard*	*None*	*Basic*	8.361	6.131
3	*None*	*None*	*Standard*	9.535	6.021	35	*Standard*	*None*	*Standard*	8.215	5.879
4	*None*	*None*	*Premium*	9.469	5.903	36	*Standard*	*None*	*Premium*	8.138	5.756
5	*None*	*Basic*	*None*	9.868	6.476	37	*Standard*	*Basic*	*None*	8.586	6.355
6	*None*	*Basic*	*Basic*	9.549	5.790	38	*Standard*	*Basic*	*Basic*	8.216	5.645
7	*None*	*Basic*	*Standard*	9.420	5.539	39	*Standard*	*Basic*	*Standard*	8.065	5.385
8	*None*	*Basic*	*Premium*	9.352	5.416	40	*Standard*	*Basic*	*Premium*	7.986	5.257
9	*None*	*Standard*	*None*	9.833	6.322	41	*Standard*	*Standard*	*None*	8.541	6.197
10	*None*	*Standard*	*Basic*	9.513	5.629	42	*Standard*	*Standard*	*Basic*	8.168	5.480
11	*None*	*Standard*	*Standard*	9.383	5.375	43	*Standard*	*Standard*	*Standard*	8.016	5.218
12	*None*	*Standard*	*Premium*	9.315	5.252	44	*Standard*	*Standard*	*Premium*	7.935	5.088
13	*None*	*Premium*	*None*	9.800	6.171	45	*Standard*	*Premium*	*None*	8.497	6.043
14	*None*	*Premium*	*Basic*	9.478	5.472	46	*Standard*	*Premium*	*Basic*	8.122	5.319
15	*None*	*Premium*	*Standard*	9.347	5.216	47	*Standard*	*Premium*	*Standard*	7.968	5.054
16	*None*	*Premium*	*Premium*	9.279	5.091	48	*Standard*	*Premium*	*Premium*	7.886	4.924
17	*Basic*	*None*	*None*	8.701	7.089	49	*Premium*	*None*	*None*	8.624	6.545
18	*Basic*	*None*	*Basic*	8.338	6.405	50	*Premium*	*None*	*Basic*	8.252	5.846
19	*Basic*	*None*	*Standard*	8.192	6.156	51	*Premium*	*None*	*Standard*	8.102	5.589
20	*Basic*	*None*	*Premium*	8.114	6.034	52	*Premium*	*None*	*Premium*	8.023	5.464
21	*Basic*	*Basic*	*None*	8.561	6.626	53	*Premium*	*Basic*	*None*	8.483	6.073
22	*Basic*	*Basic*	*Basic*	8.190	5.925	54	*Premium*	*Basic*	*Basic*	8.104	5.356
23	*Basic*	*Basic*	*Standard*	8.038	5.667	55	*Premium*	*Basic*	*Standard*	7.948	5.092
24	*Basic*	*Basic*	*Premium*	7.959	5.541	56	*Premium*	*Basic*	*Premium*	7.867	4.963
25	*Basic*	*Standard*	*None*	8.514	6.470	57	*Premium*	*Standard*	*None*	8.437	5.913
26	*Basic*	*Standard*	*Basic*	8.140	5.762	58	*Premium*	*Standard*	*Basic*	8.055	5.190
27	*Basic*	*Standard*	*Standard*	7.988	5.501	59	*Premium*	*Standard*	*Standard*	7.897	4.923
28	*Basic*	*Standard*	*Premium*	7.907	5.374	60	*Premium*	*Standard*	*Premium*	7.815	4.794
29	*Basic*	*Premium*	*None*	8.470	6.318	61	*Premium*	*Premium*	*None*	8.392	5.759
30	*Basic*	*Premium*	*Basic*	8.093	5.604	62	*Premium*	*Premium*	*Basic*	8.007	5.029
31	*Basic*	*Premium*	*Standard*	7.939	5.341	63	*Premium*	*Premium*	*Standard*	7.848	4.758
32	*Basic*	*Premium*	*Premium*	7.857	5.212	64	*Premium*	*Premium*	*Premium*	7.765	4.628

Appendix C

The branch-and-cut algorithm is derived from the branch-and-bound algorithm combined with the cutting plane method [53], whose flowchart is presented in Fig. C1.

Initialization
Add MILP to active node L $\overline{z} \leftarrow +\infty$ $\underline{z} \leftarrow -\infty$

Problem Selection
Select and delete MILP^l, $l \in L$

Relaxation
Compute the optimal solution to LP relaxation of MILP^l, $\underline{z}_q \leftarrow -z^{lR}$

Add Cutting Planes
If desired, search for cutting planes that are violated x^{lR}

Cuts added ? — Yes / No

Is it feasible ? — Yes / No

$\underline{z}_q \leftarrow +\infty$

$\underline{z}_q \geq \overline{z}$? — Yes / No

Is x^{lR} integer ? — Yes / No

Delete from L all problems $\overline{z} \leftarrow \underline{z}_q$

Partitioning
Add problems $\left\{ \text{MILP}^{lj} \right\}_{j=1}^{j=k}$ to L

$L \neq \Phi$? — Yes / No

Termination
Stop and output x^* and $\overline{z}$

Nomenclature
$\overline{z}$: upper bound
$\underline{z}_q$: lower bound
x^{lR} : solution of LP relaxation
z^{lR} : objective value of relaxation
x^* : incumbent solution
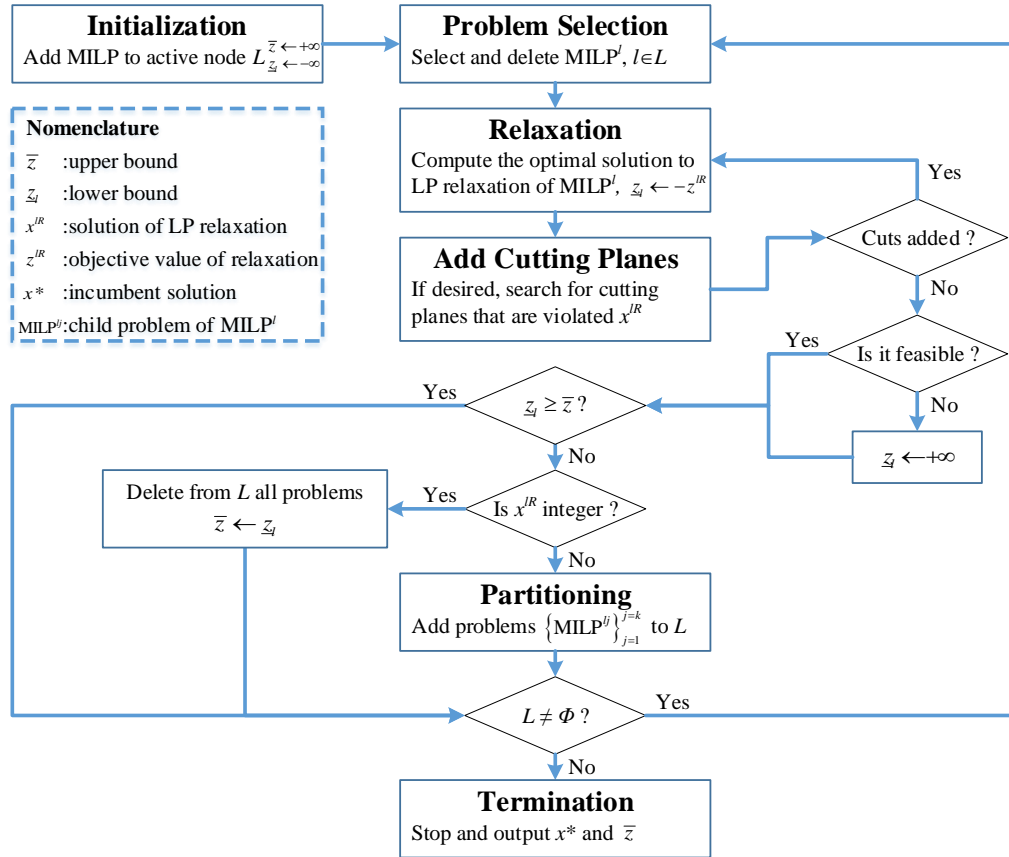MILP^{lj} : child problem of MILP^l

Fig. C1. Flowchart of the branch-and-cut algorithm used in this study.